Journal of Geosciences, 71 (2026), 39–56 DOI: 10.3190/jgeosci.0062.26

Original paper

Late fibrous tourmaline from granitic pegmatites enclosed in compositionally contrasting Mg- and Ca,Mg-rich rocks; a monitor of late external fluids

Ivo MACEK[1,2*], Milan NOVÁK[1], Petr GADAS[1], Petr BAČÍK[3,4], Michaela VAŠINOVÁ-GALIOVÁ[5]

[1] *Department of Geological Sciences, Faculty of Natural Sciences, Masaryk University, Kotlářská 2, 611 37 Brno, Czech Republic*
[2] *Museum of Prague, Kožná 1, 110 00 Praha 1, Czech Republic*
[3] *Department of Mineralogy, Petrology and Economic Geology, Faculty of Natural Sciences, Comenius University in Bratislava, Ilkovičova 6, 842 15 Bratislava, Slovak Republic*
[4] *Earth Science Institute, Slovak Academy of Sciences, Dúbravská cesta 9, 845 28 Bratislava, Slovak Republic*
[5] *Institute of Chemistry and Technology of Environmental Protection, Brno University of Technology, 612 00 Brno, Czech Republic*
[*] *Corresponding author*

Late fibrous tourmalines from three granitic pegmatites with similar size, internal structure and compositionally contrasting Mg- and Mg,Ca-rich host rocks (serpentinite – barren pegmatite Dolní Bory North, dolomite-calcite marble +calc-silicate rock – elbaite-subtype pegmatite Bližná I, both localities in Czech Republic, and spodumene-subtype pegmatite Tamponilapa Ambany, Sahatany Valley, Madagascar) were examined. We focused on their morphology, zonal patterns, chemical composition (EMPA, LA-ICP-MS), powder XRD and RAMAN spectroscopy as well as on the chemical composition of the associated early tourmalines (schorl – Dolní Bory, Mg-rich liddicoatite-elbaite – Bližná, dravite-schorl – Tamponilapa) to reveal textural and compositional relations. Fibrous tourmalines are Mg-rich and F- and Ca-poor: Dolní Bory – greyish Fe-rich dravite with Al_{tot} 6.07–6.33 *apfu*, Mg 1.45–1.62 *apfu*, Fe_{tot} 0.97–1.26 *apfu*; Bližná – blue to colorless dravite with Al_{tot} 6.15–6.36 *apfu*, Mg 1.97–2.22 *apfu*, Fe_{tot} 0.20–0.34 *apfu*; Tamponilapa – colorless to brownish dravite–oxy-dravite and rare magnesio-foitite with Al_{tot} 6.42–6.77 *apfu*, Mg 1.78–2.23 *apfu*, Fe_{tot} 0.16–0.24 *apfu*; low Ca ≤ 0.13 *apfu*, moderate *X*-site vacancy 0.31–0.51 *pfu*, very low F ≤ 0.01 *apfu* (Dolní Bory, Tamponilapa) are typical. The contents of major, minor and trace elements manifest that the following factors play a substantial role for composition of fibrous tourmalines: external fluids from host rocks with contrasting chemistry (e.g., Mg, Cr, Ni, V), internal residual fluids from pegmatite (H_2O, B, Li, Si, Al), and the chemical compositions of early tourmalines (B, Si, Al, Fe). Fibrous habitus of tourmalines was facilitated by crystallization from low-T aqueous fluids and controlled chiefly by crystal-structural constraints and rate of crystallization. The complex textural relations do not allow to reliably define their origin – direct replacement of early tourmaline, its overgrowing after its partial dissolution or combination of both processes.

Keywords: late fibrous tourmaline, dravite, habitus, chemical composition, granitic pegmatite, Mg,Ca-rich host rocks
Received: January 21, 2026; accepted: September 3, 2026; handling editor: F. Bosi

1. Introduction

Fibrous and acicular tourmalines occur in a variety of low-T geological environments. They are typically nucleated on a single pre-existing tourmaline crystal or on other minerals in fluid-filled space and a presence of abundant aqueous fluids is essential (Dutrow and Henry 2016). Fibrous and acicular tourmalines are known from a variety of hydrothermal veins (e.g., Rosenberg and Foit 2006; Bačík et al. 2015; Dutrow and Henry 2016), geothermal systems (Moore et al. 2004), authigenic overgrowths of tourmaline in diverse metasediments (e.g., Van Dem Bleeken et al. 2007; Henry and Dutrow 2012), and chiefly from granitic pegmatites (e.g., Pezzotta et al. 1996; Novák 1998; Dutrow and Henry 2000, 2016; Novák and Taylor 2000; Novák et al. 2017; Andreozzi et al. 2025). Fibrous tourmaline is typically a sole mineral of the late assemblages and the low-T conditions T < ~300 °C are considered in some localities (e.g., Novák and Taylor 2000; Henry and Dutrow 2012; Bačík et al. 2015). They are compositionally highly variable showing dravitic, foititic, schorlitic and elbaitic compositions (Dutrow and Henry 2016). Single crystals are homogeneous or heterogeneous with a variety of irregular, patchy and oscillatory zoning (Dutrow and Henry 2016 and references therein). Due to the compatibility of tourmaline with many elements fibrous tourmalines are considered a useful recorder of chemical composition of late aqueous fluids (Dutrow and Henry 2016).

Fibrous to acicular tourmalines were described from several granitic pegmatites worldwide (e.g., Pezzotta et al. 1996; Aurisicchio et al. 1999; Novák and Taylor

Published under Creative Commons Attribution-NonCommercial 4.0 International (CC BY-NC 4.0) license

Tab. 1 Geological setting and mineral assemblages of the examined granitic pegmatites. 1 – Staněk (2009), 2 – Novák et al. (1999), 3 – Novák et al. 2012, 4 – Radková et al. (2021), 5 – Buřival and Novák (2018), 6 – Novák et al. (2025). The abbreviations of minerals according to Warr (2021).

Locality	Geology			Minerals				Source
	pegmatite		host rock	reaction rim with host rock	major	minor	primary tourmaline	selected accessory	
Dolní Bory North	barren	subvertical nest, ~3 m thick	serpentinite	unknown	Kfs+Plg+Qz	Tur+Bt+Ab	Srl	Grt, Ap, Zrc, Col, Mic	1
Bližná I	mixed LCT-NYF elbaite-subtype	subvertical dike, 35° SE, 3–4 m thick ~50 m long	Dol-Cal marble, calc-silicate rock	locally Tur+Ax	Kfs+Plg+Qz+Ab	Tur	Srl, Uvt, Drv, Elb, Ld, Fld, Felb	Zrc, Ttn, Flr, Aln-Ce, Bsn-Ce, Di, Dat, Cal, Ax-Mn, Ax-Mg, Ap, Mic	2, 3, 4
Tamponilapa Ambany	LCT spodumene-subtype	subhorizontal dike ~5 m thick ~150 m long	Dol-Cal marble, calc-silicate rock	commonly Tur+Di locally Tur+Hlm+Spd	Kfs+Plg+Qz+Ab	Tur+Spd+Bt+Hlm	Srl, Drv, Odrv, Fev, Osc, Elb, Fel, Mfo, Ld	Sps, Brl, Dbu, Fhlm, Ax-Fe, Zrc, Col, Mic, Cst, Tpz, Ap, Mag, Rt	5, 6

2000; Dutrow and Henry 2000, 2016 and references therein; Felch et al. 2016; Andreozzi et al. 2025). Several paragenetic types of fibrous tourmaline were recognized in granitic pegmatites of the Moldanubian Zone: blue Fe-rich elbaite to fluor-elbaite replacing garnet (e.g., Němec 1989; Buřival and Novák 2018), blue dravite replacing cordierite (Novák 1998), black to dark violet foitite overgrowing fluor-elbaite in a miarolitic pocket (Novák and Taylor 2000) and grey, brown to colorless dravite and magnesio-foitite overgrowing early tourmaline (dravite, schorl, oxy-schorl) from miarolitic pockets in simple granitic pegmatites (Gadas et al. 2012; Novák et al. 2017).

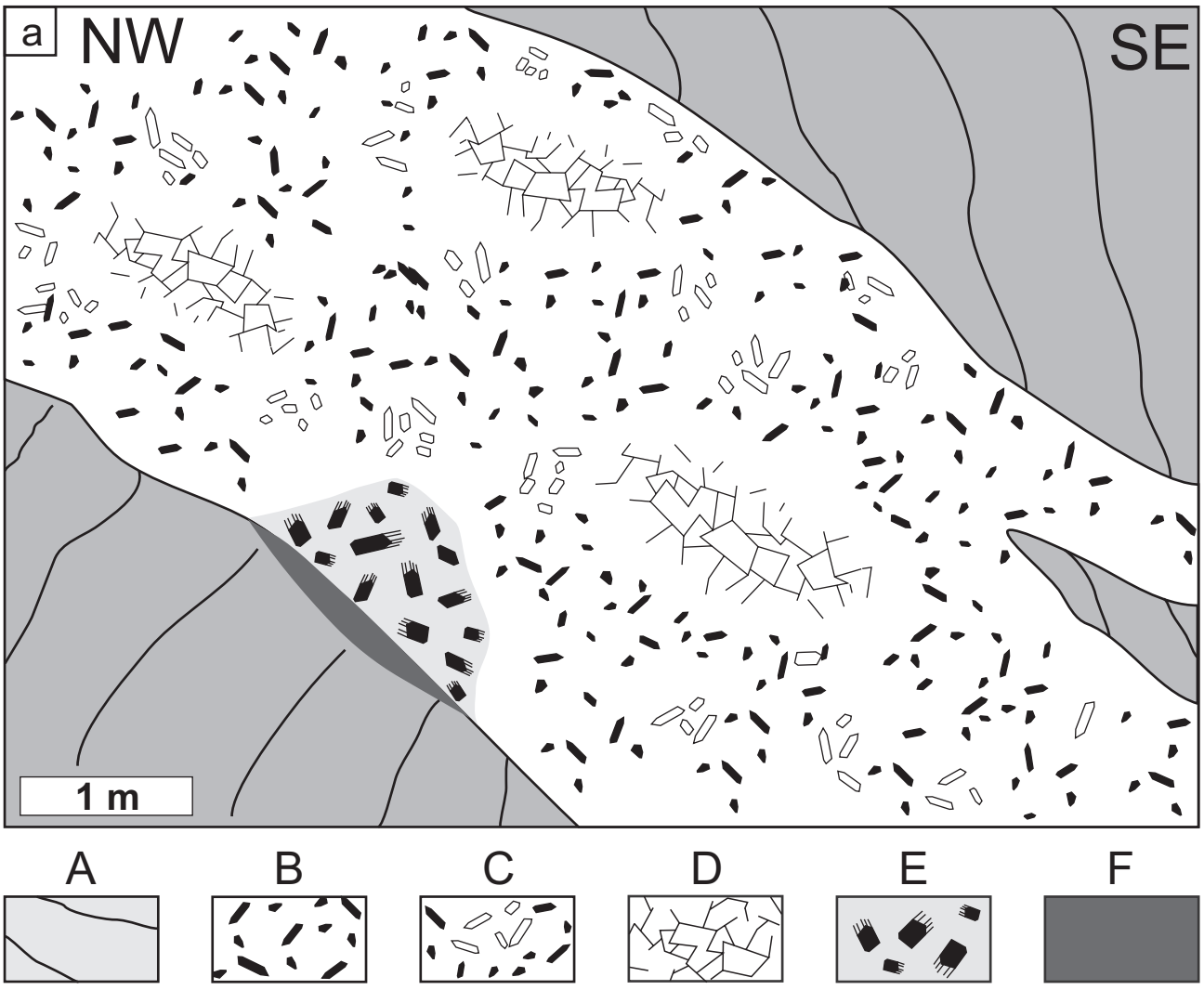
We examined in detail fibrous tourmalines from three granitic pegmatites with similar size, internal structure and compositionally contrasting Mg- and Mg,Ca-rich host rocks (serpentinite, dolomite-calcite marble, calc-silicate rock). They differ in the degree of fractionation from primitive barren pegmatite Dolní Bory North (Staněk 2009; Novák et al. 2017) to Li-enriched elbaite-subtype pegmatite Bližná I (Novák et al. 1999, 2012) both from the Moldanubian Zone, Czech Republic, and spodumene-subtype pegmatite Tamponilapa Ambany, Sahatany Valley, Madagascar (Ranorosoa 1986; Buřival and Novák 2018; Novák et al. 2025). We focused on textural position, morphology, zonal patterns, mineral assemblages, chemical composition (EMPA, LA-ICP-MS), RAMAN spectroscopy and powder XRD of fibrous tourmalines to reveal compositional evolution relative to the early tourmalines, a role of contrasting chemistry of host rocks and related external fluids, a role of internal residual fluids and potential crystal-structural constraints on chemical composition of tourmalines.

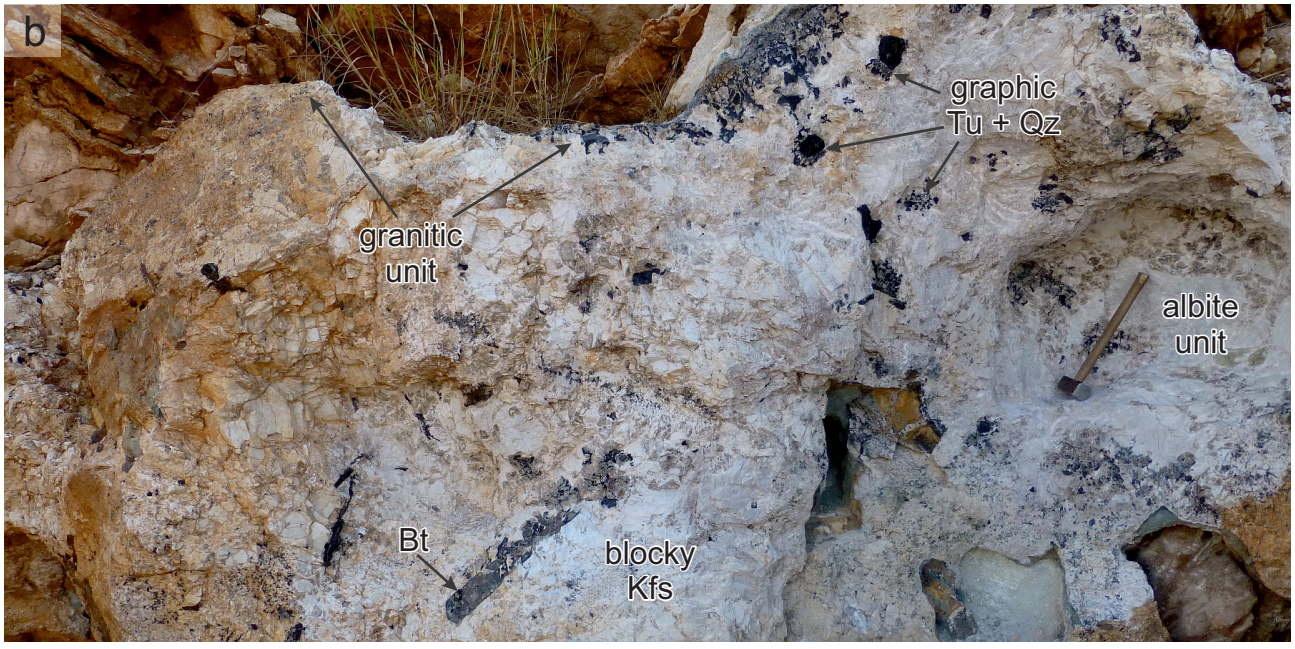
2. Geological setting of granitic pegmatites

The studied pegmatites occur in high- to medium-grade metamorphic rocks of the Moldanubian Zone, Bohemian Massif, Czech Republic (e.g., Schulmann et al. 2014 and references therein) or in low- to medium-grade metamorphic rocks of the Itremo Complex, Central Madagascar (e.g., Cox et al. 1998; Moine et al. 2014). They form subvertical and subhorizontal bodies, 3 to 5 m thick (Tab. 1) with reaction rims developed locally on the contact with the host rock in available outcrops.

⇨

Fig. 1 Internal structure of the selected examined pegmatites. **a –** Cross section through the Bližná I pegmatite; A – host rock, B – schorl unit, C – elbaite–liddicoatite unit, D – diopside-bearing nests, E – uvite–liddicoatite unit host of the examined primary and fibrous tourmalines, F – narrow tourmaline-rich contact zone (modified from Novák et al. 1999); **b –** Tamponilapa Ambany pegmatite.


a
NW
SE
1 m
A
B
C
D
E
F


b
graphic
Tu + Qz
granitic
unit
albite
unit
Bt
blocky
Kfs

The pegmatite dike Dolní Bory North located in the Bory Granulite Massif region is known from abundant large fragments in the agricultural field and poor outcrops (Staněk 2009; Macek 2012). It exhibits heterogeneous internal structure consisting of the following textural-paragenetic units: (i) medium- to coarse-grained granitic unit (Kfs + Plg + Qz ± + Bt) typically on the border zone, (ii) graphic unit (Kfs + Qz ± Bt) locally with tourmaline+quartz graphic intergrowths, (iii) blocky K-feldspar, and minor (iv) medium- to coarse-grained albite unit (Ab + Qz + Kfs + Tur ± Grt). The latter three units are rather randomly distributed within the pegmatite body. Quartz from the graphic unit is locally dissolved and open space was scarcely filled by late greenish opal. Biotite is locally replaced by black tourmaline (Macek 2012). The contact with host serpentinite is strongly weathered.

The Bližná I pegmatite dike cuts silicates-rich dolomite-calcite marbles (Radková et al. 2021) at the abandoned graphite Mine Václav, Bližná near Černá v Pošumaví. It has complex internal structure (Fig. 1a; Novák et al. 1999, 2012) consisting of volumetrically dominant (i) coarse- to medium-grained schorl unit (Kfs + Ab + Qz + Tur) evolving gradually into minor nests of (ii) elbaite-liddicoatite-bearing unit (Kfs + Ab + Qz + Tur ± Di), up to 30 cm in diameter. (iii) Graphic unit (Kfs + Qz) and (iv) blocky K-feldspar are only locally present in the dominant (i) schorl unit. An isolated nest of (v) uvite-liddicoatite unit (Plg > Kfs + Qz + Tur ± Cal), 1 × 1.5 m in diameter, is developed along the footwall contact (Fig. 1a) and it has coarse-grained granitic texture. The contacts of pegmatite with host rocks are typically sharp, only scarcely, a thin zone of diopside + rare tremolite is developed. Tourmaline-rich exocontact zone, up to 20 cm thick and 1.5 m long, with abundant Li,F-enriched dravite–uvite + elbaite–liddicoatite + axinite-(Fe) is restricted on the footwall pegmatite margin adjacent to the spatially limited (v) uvite-liddicoatite unit (Novák et al. 1999, 2012; Krmíček et al. 2021) (Fig. 1a) with blue to colorless fibrous dravite examined. Primary tourmalines from this unit (uvite, liddicoatite–elbaite) are typically Mg-enriched (Novák et al. 1999). Fibrous tourmaline has not been observed in other volumetrically dominant pegmatite units.

The Tamponilapa Ambany pegmatite (Ranorosoa 1986; Buřival and Novák 2018; Novák et al. 2025) has very heterogeneous internal structure consisting of the following textural-paragenetic units: (i) medium- to coarse-grained granitic unit (Kfs + Plg + Qz ± Bt) typically on the border zone, (ii) rare graphic unit (Kfs + Qz ± Bt) locally within tourmaline + quartz and rare garnet + quartz graphic intergrowths (Fig. 1b), (iii) blocky K-feldspar (locally amazonite), and (iv) medium- to coarse-grained (cleavelandite) albite unit (Ab + Qz + Tur) with locally abundant spodumene laths, up to ~20 cm long. Biotite randomly distributed with the pegmatite body is locally replaced by fibrous radial aggregates of dark blue ferro-holmquistite and/or blue Fe-rich elbaite (Novák et al. 2025) and garnet is replaced by blue Fe-rich elbaite (Buřival and Novák 2018). Miarolitic pockets lined with Li-tourmaline and crystals of hambergite are rare. All units except for the border granitic unit are rather randomly distributed in the pegmatite (Fig. 1b). The thin reaction zone of black Fe-rich dravite + greenish diopside is common in the available upper pegmatite contacts whereas the assemblage Fe-rich dravite + fibrous violet holmquistite to ferro-holmquistite ± spodumene occurs locally along the footwall contact (Novák et al. 2025).

The examined pegmatite bodies have similar size, rather irregular distribution of the textural-paragenetic units, rather abundant tourmalines, absence or rare to minor biotite, and absence of muscovite and lepidolite (Tab. 1). The mineral assemblages were in part triggered by an external contamination from host rocks. The Bližná I pegmatite contains diopside and rare primary REE-minerals (allanite-(Ce), bastnaesite-(Ce)) and the mixed NYF-LCT affiliation is feasible (see Novák et al. 2012), whereas the Tamponilapa Ambany pegmatite exhibits an evident LCT affiliation. The barren pegmatite Dolní Bory N is primitive, and its affiliation is not possible to assess consistently. Also, exocontact reaction zones with tourmalines, diopside, axinite, and/or holmquistite developed between the (v) uvite-liddicoatite pegmatite unit in the Bližná I pegmatite and in the upper and footwall contact at the Tamponilapa Ambany pegmatite are typical. For more details about internal structure, mineralogy, geochemistry and origin of the individual pegmatites see Staněk (2009), Novák et al. (1999, 2012, 2017), Krmíček et al. (2021), Ranorosoa (1986), Buřival and Novák (2018) and (Novák et al. 2025).

3. Methods

3.1. Sampling

The samples examined were obtained from the mineral collection of the Moravian Museum, Brno and collected by the authors at the individual localities (Tab. 2). We used the following abbreviations for the description purposes to recognize distinct types of early and late tourmalines: (a) position in the pegmatite evolution: E – early, I – intermediate, L – late; (b) tourmaline species: D – dravite, S – schorl, E – elbaite, L – liddicoatite; (c) locality: DB – Dolní Bory N, Bl – Bližná, Ta – Tamponilapa Ambany; examples: early schorl from Dolní Bory (E-S-DB), late dravite from Bližná I (L-D-Bl) and intermediate elbaite from Tamponilapa (I-E-Ta). The abbreviations of minerals given in the text, tables and figures are used according to Warr (2021).

Tab. 2 Description of fibrous tourmalines.

sample	morphology	length of fibers	color	associated minerals	source of samples
(L-D-DB)	subparallel fibers	≤6 mm	greyish	opal CT	sample A 4258, Moravian Museum, Brno
(L-D-Bl)	massive to prismatic to subparallel fibers	≤3 mm	bluish to colorless	quartz K-felspar	graphite Mine Václav, collected by M. Novák 1994
(L-D-Ta)	fibers parallel to c-axes of early Tur, hair-like aggregates	≤~20 mm	bluish to colorless to brownish	albite	pegmatite outcrop, collected by I. Macek, M. Novák 2012, 2022

3.2. EMPA

The compositions of the minerals were determined using a Cameca SX100 electron microprobe in the Laboratory of Electron Microscopy and Microanalysis, Department of Geological Sciences, Faculty of Science, Masaryk University, Brno. Analyses were carried out in the wavelength dispersive mode, with an accelerating voltage of 15 kV, a beam current of 10 nA and a spot size ~5 μm. The following standards and X-ray Kα lines were used: sanidine (Si, Al, K); albite (Na); olivine (Mg); wollastonite (Ca); almandine (Fe); spessartine (Mn); fluorapatite (P); titanite (Ti); chromite (Cr); topaz (F); gahnite (Zn); $SrSO_4$ (S); $ScVO_4$ (V, Sc); synthetic Rb-silicate (Rb); and pollucite (Cs). The peak counting time was 10 s for major elements and 20–40 s for minor to trace elements. The background counting time was half of the peak counting time at the high- and low-energy background positions each. Raw intensities were corrected for matrix effects using the X-PHI algorithm (Merlet 1994). The theoretical amount of unanalysed light elements (H, Be, B and O) was included in the matrix correction.

3.3. LA-ICP-MS

Contents of the trace elements were obtained using three different LA-ICP-MS instrumentation setups. A double focusing ICP-MS Element 2 Thermo Scientific™ coupled to an Analyte G2 laser ablation system (Teledyne CETAC Technologies) equipped with ArF* excimer laser operating at a wavelength of 193 nm and installed at the Department of Chemistry, Masaryk University Brno. The second instrumentation housed at Faculty of Chemistry, Brno University of Technology and BIC Brno, consists of ArF* excimer laser ablation system Analyte Excite+ (Teledyne CETAC Technologies,), emitting the laser beam at a wavelength of 193 nm, was connected to quadrupole ICP mass spectrometer Agilent 7900 (Agilent).

3.4. Raman spectroscopy

Raman spectra were measured with Thermo Scientific's Raman dispersion spectrometer – the DXR Microscope model, which is equipped with an Olympus confocal microscope. An Nd:YAG diode laser with a wavelength of 532 nm and an input power of 10 mW served as an excitation source. A grid of 400 notches/mm was used. A multi-channel thermoelectrically cooled CCD camera served as a detector. The samples were measured at 50× magnification with a measuring trace of about 1 μm^2 and through an aperture of 50 μm pinhole. Only the needle-like phases of the sample from Dolní Bory were measured through the 25 μm pinhole aperture to increase the spatial resolution (filtering out the Raman spectrum of the surrounding fixing resin). The measurements were carried out at a power of 9 mW, a measuring time of 20 s and with 10 accumulations of spectrum at the University of Chemistry and Technology in Prague.

3.5. XRD

X-ray powder diffraction data were obtained using a Bruker D8 Advance powder diffractometer (National Museum, Prague) with a semiconductor position-sensitive LynxEye detector using CuKα radiation (40 kV, 40 mA). Powder preparations were applied in acetone suspension to a carrier made of a single crystal of silicon and subsequently diffraction data were obtained in step-scanning mode (step 0.01o, reading time 8 s/detector step, total experiment time approx. 15 hours). The positions of the individual diffraction maxima were described by the Pseudo-Voigt profile function and refined by profile fitting in the HighScore Plus program. The lattice parameters were refined using the least squares method using the Celref program (Laugier and Bochu 2011).

4. Results

4.1. Textural and paragenetic position of fibrous dravite

The individual late fibrous dravites from the examined localities were nucleated exclusively on early tourmaline but they are rather different in their host pegmatite unit, color and morphology (Tab. 2).

Grey fibrous dravite from Dolní Bory N (L-D-DB) is ongrowing large prismatic crystal of black schorl (E-S-DB) from blocky unit and the contact with early tourmaline is typically straight and sharp (Fig. 2a). It is penetrated by numerous veinlets of opal-CT (Novák et

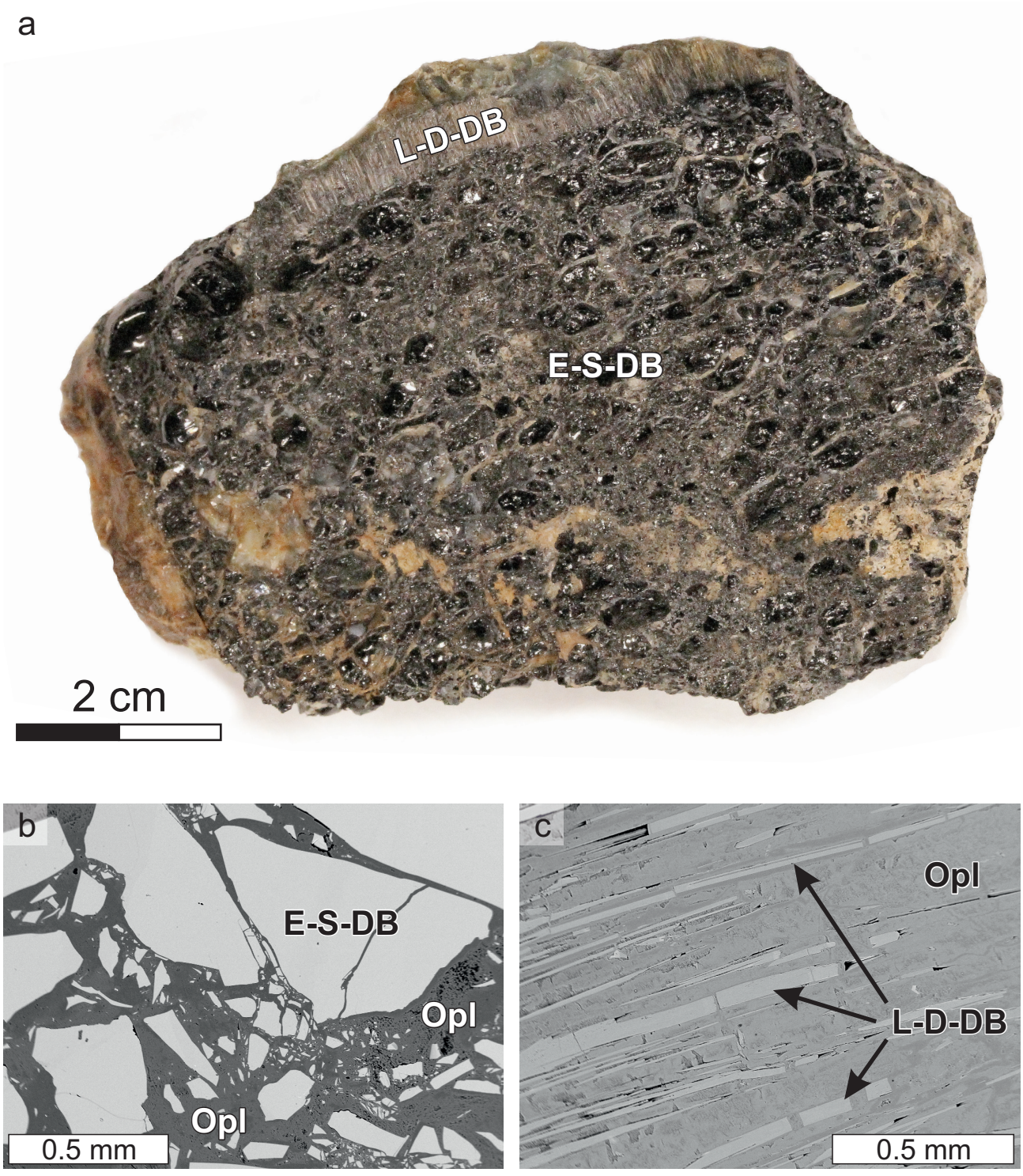


Fig. 2 Dolní Bory North. **a** – macro photo of tourmaline aggregate (photo J. Toman); **b** – fragments of early tourmaline (E-S-DB) in opal; **c** – fragments of fibrous tourmaline (L-D-DB) in opal matrix.

al. 2017) which form a matrix of the early tourmaline (E-S-DB) fragments and opal also is interstitial among individual fibers of late dravite (L-D-DB) (Fig. 2b, c). Mutual orientation of early tourmaline (E-S-DB) and late fibres (L-D-DB) is not apparent.

Blue to colorless prismatic to fibrous dravite from Bližná I (L-D-Bl) is overgrowing crystals of zoned pale brown Mg-enriched liddicoatite-elbaite (E-LE-Bl) (Fig. 3a) exclusively from the (v) uvite-liddicoatite unit (Fig. 1a). The fibrous texture of dravite is developed only

locally as thin veinlets on fractures of early pale brown tourmaline (E-LE-Bl) or fibers are growing on crystal terminations mostly into the host massive quartz (Fig. 3). Early tourmaline (E-LE-Bl) and fibrous tourmaline (L-D-Bl) show evidently the same crystal orientation.

Early black Fe-rich dravite to Mg-rich schorl (E-DS-Ta) from Tamponilapa Ambany forms prismatic crystals, up to ~15 cm long, in the albite unit (Fig. 4a) located close to the upper contact. It is oscillatory zoned (Fig. 4b) and frequently porous after strong alteration. Colorless subparallel to colorless and brownish hair-like aggregates of fibrous dravite to oxy-dravite from Tamponilapa Ambany (L-D-Ta) occur on prismatic crystals of early black tourmaline (E-DS-Ta) and crystallized into secondary open space likely after the dissolution of early tourmaline. A narrow intermediate zone of blue to bluish Fe-enriched elbaite (I-E-Ta) is often developed between early black dravite-schorl (E-DS-Ta) and colorless fibrous dravite (L-D-Ta) (Fig. 4). Early tourmaline (E-DS-Ta), intermediate tourmaline (I-E-Ta) and early generation of fibrous tourmaline (L-D-Ta) show evidently the same crystal orientation whereas the latest hair-like tourmaline is chaotic.

4.2. Chemical composition

4.2.1. EMPA

The chemical compositions of early tourmalines from the individual localities differ significantly (Tab. 3, Fig. 5). In the pegmatite Dolní Bory N black Al-poor schorl (E-S-DB) yielded low Al_{tot} 5.28–5.97 *apfu*, variable Mg 0.63–1.23 *apfu* and Fe_{tot} 1.99–2.47 *apfu*, Na 0.76–0.87 *apfu*, and low Ca ≤0.12 *apfu* (Fig. 5a, b). Aggregates of liddicoatite-elbaite (E-LE-Bl) from the pegmatite Bližná I gave Al_{tot} 6.68–6.91 *apfu*, Mg 0.30–0.76 *apfu*, very low Fe_{tot} 0.04–0.11 *apfu*, Na 0.43–0.71 *apfu*, and Ca 0.23–0.49 *apfu*, (Fig. 5c, d). Black oscillatory zoned Fe-rich dravite to Mg-rich schorl to rare fluor-dravite (E-DS-Ta) from Tamponilapa Ambany is very heterogeneous (Fig. 5e, f). It yielded low to moderate Al_{tot} 5.65–6.32 *apfu*, highly variable Mg 0.65–2.32 *apfu* and Fe_{tot} 0.49–2.37 *apfu*, Na 0.51–0.74 *apfu*, Ca 0.17–0.46 and F 0.16–0.72 *apfu*. A narrow intermediate zone of Fe-rich elbaite (I-E-Ta) developed between early primary dravite to schorl (E-DS-Ta) and late fibrous dravite (L-D-Ta) has Al 7.10–7.23 *apfu*, low Mg 0.17–0.24

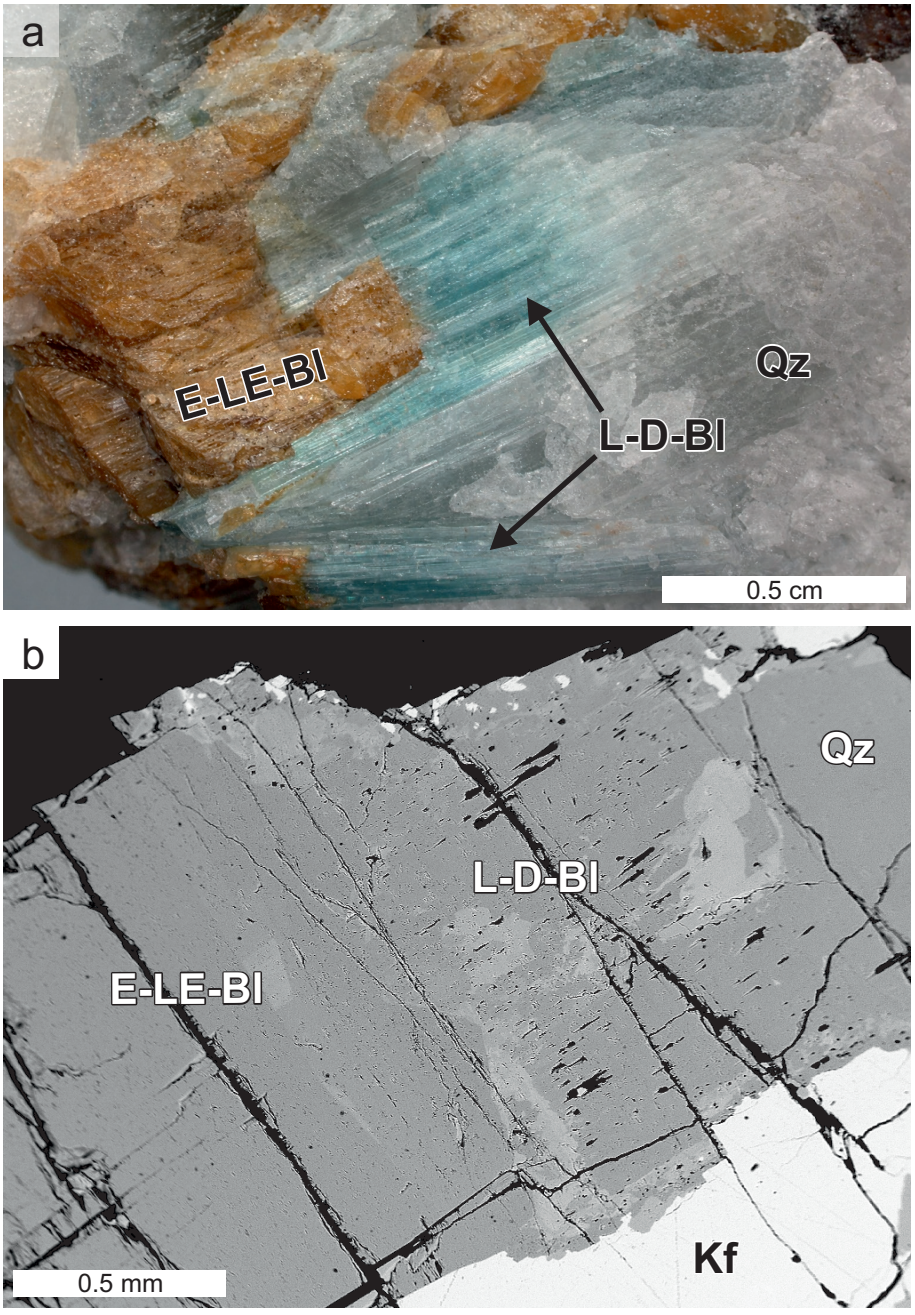


Fig. 3 Bližná I. **a** – Macro photo and **b** – BSE image of early tourmaline (E-LE-Bl) and fibrous tourmaline (L-D-Bl) in quartz.

apfu, Fe 0.56–0.88 *apfu*, Na 0.58–0.62 *apfu* and low Ca 0.08–0.10 *apfu*. Low Mn 0.09–0.13 *apfu* and F 0.09–0.13 *apfu* were also detected in early tourmalines from Dolní Bory N and Bližná I whereas F is highly variable in Tamponilapa Ambany.

Chemical compositions of fibrous tourmalines are evidently less variable compared to the early ones (Fig. 5, Tab. 3). In the Dolní Bory N pegmatite, Fe-rich dravite (L-D-DB) gave Al_{tot} 6.07–6.33 *apfu*, Mg 1.45–1.62 *apfu*, rather high Fe_{tot} 0.97–1.26 *apfu*, (Fig. 5b). Blue to colorless dravite (L-D-Bl) from Bližná I yielded Al_{tot} 6.15–6.36 *apfu*, Mg 1.97–2.22 *apfu*, Fe_{tot} 0.20–0.34 *apfu*, Na 0.49–0.61 *apfu*, Ca 0.04–0.13 *apfu*. Fibrous dravite to oxy-dravite and rare magnesio-foitite from Tamponilapa (L-D-Ta) showed Al_{tot} 6.42–6.77 *apfu*, Mg 1.78–2.23 *apfu*, Fe_{tot} 0.16–0.24 *apfu*, very low Ca ≤ 0.01 and vacancies in the X-site position in the range of 0.31–0.51 *pfu* (Fig. 5e). The contents of F are very low ≤ 0.01 *apfu* in all examined samples of late fibrous tourmalines from Dolní Bory and Tamponilapa but slightly higher in Bližná F ≤ 0.17 *apfu*.

4.2.2. Trace elements LA-ICP-MS in late fibrous dravite

Samples of fibrous dravite were analyzed using LA-ICP-MS to reveal concentrations of trace elements active in late stages of a pegmatite evolution. The individual analyses of dravite (L-D-DB) from the Dolní Bory N (Novák et al. 2017) show significantly different concentrations of trace elements compared to the late fibrous tourmalines in Bližná I (L-D-Bl) and Tamponilapa Ambany (L-D-Ta) (Fig. 6). The major differences were found in the concentrations of Cr (104–937 ppm) and Ni (106–335 ppm), Ti (178–716 ppm) and V (232–448 ppm), in Dolní Bory N comparing the sample (L-D-Bl) from Bližná I (Ti 30–112 ppm, V 20–25 ppm Cr and Ni below the detection limit) and the sample (L-D-Ta) from Tamponilapa (Ti 62–213 ppm, V, Cr and Ni below the detection limit). The concentrations of Li increase from Dolní Bory N (L-D-DB) (57–157 ppm) via Bližná I (L-D-Bl) (137–406 ppm) to Tamponilapa Ambany (L-D-Ta) (442–727 ppm). In contrast, the concentrations of Mn show nearly identical values at all localities – (L-D-DB; 438–752 ppm), (L-D-Ta; 345–676 ppm), and (L-D-Bl; 388–553).

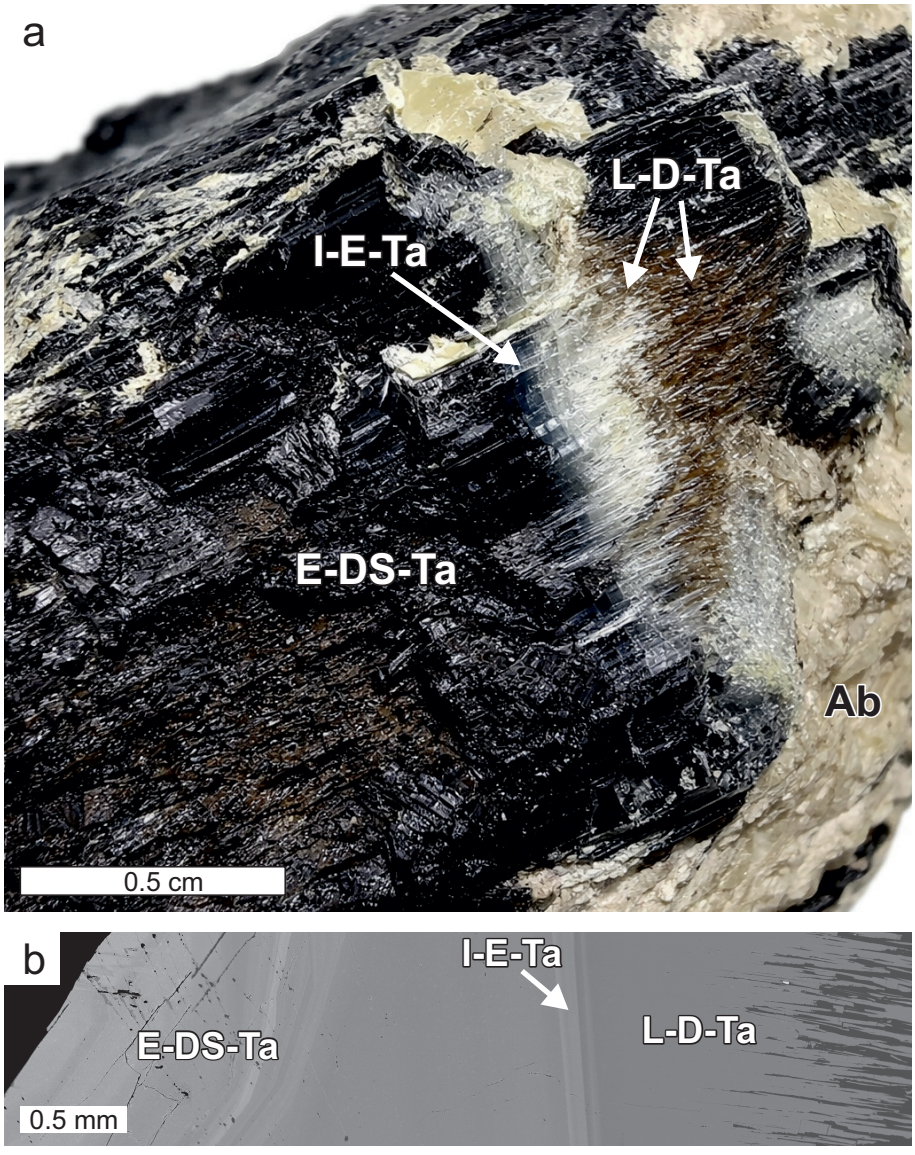


Fig. 4 Tamponilapa Ambany. **a –** Macro photo and **b –** BSE image of early (E-D-Ta), bluish intermediate tourmaline (I-E-Ta) and late multicolored fibrous tourmaline (L-D-Ta) associated with albite.

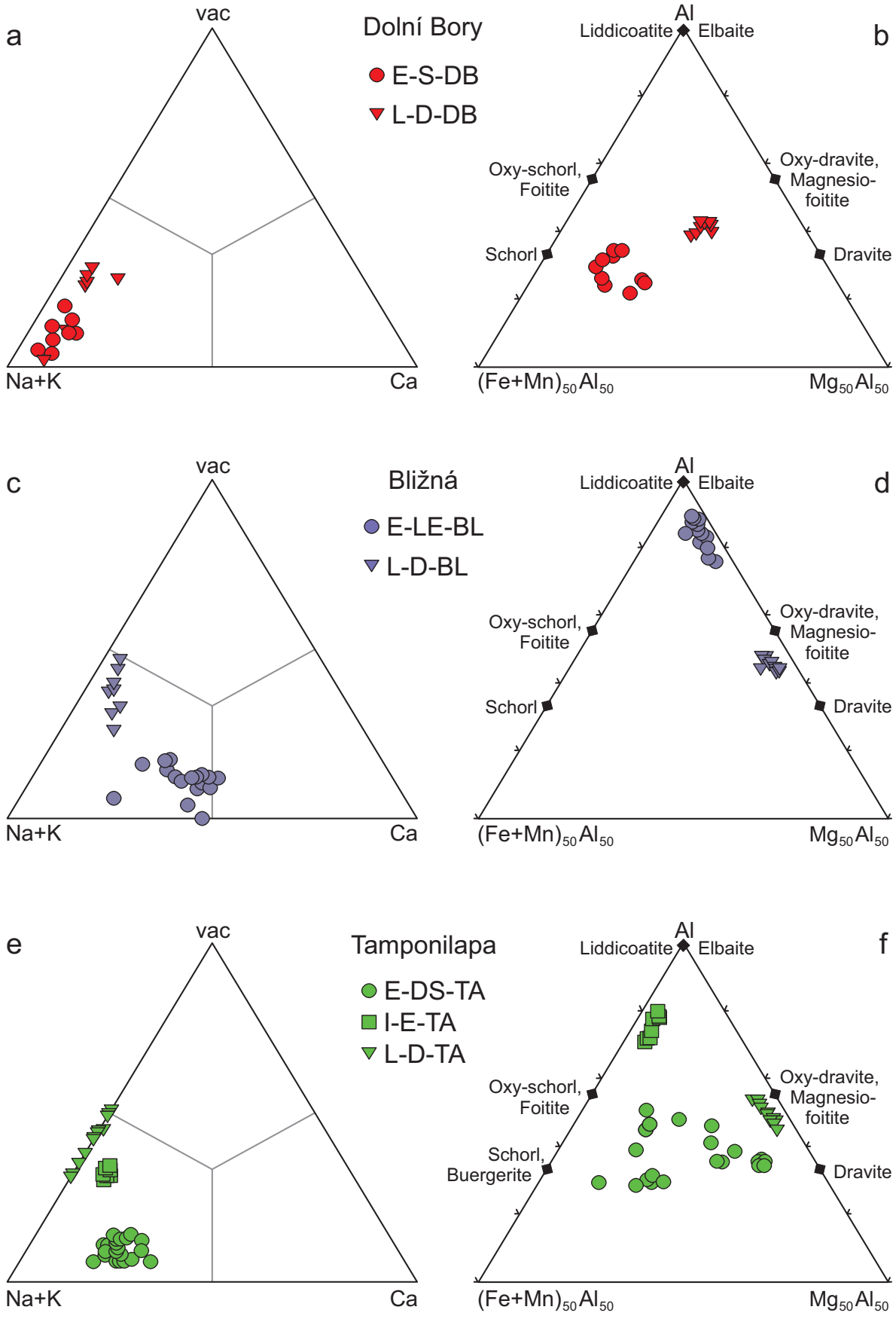
4.3. RAMAN Spectroscopy

Raman spectra of late tourmalines (L-D-DB, L-D-Bl and L-D-Ta) show the strongest vibrations in the positions 213, 238, 369, 491, 678, 708, 757, 981 and 1057 cm^{-1} in the region of 1250–150 cm^{-1} (Fig. 7). The position of the belt in the lower waveform range of 213 cm^{-1} comes from the deformation

Tab. 3 Representative chemical analyses EMP and formula calculations of studied tourmalines. Calculated on the basis of 31 anions (O, OH, F).

	E-S-DB			E-LE-Bl			E-DS-Ta			I-E-Ta			L-D-DB			L-D-Bl			L-D-Ta		
wt. %																					
SiO_2	34.89	34.66	35.11	38.39	38.47	38.18	37.08	36.98	36.26	36.67	36.84	36.81	36.96	36.92	36.98	37.75	38.38	37.87	37.79	37.83	37.78
TiO_2	0.70	0.94	1.00	0.68	0.79	1.16	0.06	0.09	0.07	0.09	0.12	0.12	0.02	0.40	0.04	0.03	0.02	0.05	b.d.l.	b.d.l.	b.d.l.
B_2O_3#	10.18	10.07	10.18	11.12	11.14	11.06	10.74	10.71	10.60	10.75	10.80	10.75	10.71	10.72	10.71	10.94	11.12	10.97	10.97	11.00	10.96
AL_2O_3	29.51	27.53	28.85	37.02	37.58	36.91	31.68	31.04	31.21	37.29	37.48	37.25	33.07	32.16	32.80	33.11	33.74	33.26	35.57	35.67	34.98
V_2O_3	0.02	0.04	0.01	b.d.l.	b.d.l.	b.d.l.	b.d.l.	b.d.l.	b.d.l.	b.d.l.	b.d.l.	b.d.l.	0.07	0.06	0.07	b.d.l.	b.d.l.	b.d.l.	b.d.l.	b.d.l.	b.d.l.
$FeO_{tot.}$	15.60	17.12	15.63	0.35	0.38	0.47	4.95	4.14	6.71	6.47	6.27	6.30	7.80	9.26	8.09	1.63	1.85	2.60	1.41	1.41	1.38
MnO	0.29	0.33	0.94	0.53	0.48	0.52	0.85	0.30	0.62	0.65	0.66	0.70	0.07	0.08	0.06	0.01	0.05	0.17	0.15	0.12	0.11
MgO	2.93	2.97	2.54	1.52	1.30	1.50	7.84	9.52	7.63	0.98	1.00	0.97	6.05	6.00	6.19	9.34	8.94	8.50	8.42	8.49	8.93
CaO	0.26	0.40	0.28	2.41	2.54	2.48	1.26	1.46	1.45	0.49	0.46	0.46	0.33	0.80	0.41	0.76	0.37	0.66	b.d.l.	b.d.l.	b.d.l.
Na_2O	2.28	2.44	2.64	1.55	1.49	1.51	2.13	2.17	2.14	1.90	1.96	1.84	2.11	1.90	2.14	1.95	1.77	1.82	1.79	1.85	2.10
K_2O	0.07	0.11	0.10	0.02	0.02	0.02	0.06	b.d.l.	0.04	b.d.l.	b.d.l.	b.d.l.	0.02	0.01	0.03	0.04	b.d.l.	0.01	b.d.l.	b.d.l.	b.d.l.
Li_2O	0.00	0.00	0.08	2.57	2.51	2.43	0.42	0.23	0.21	1.16	1.19	1.17	0.20	0.15	0.17	0.56	0.70	0.63	0.27	0.27	0.26
F	0.03	0.07	0.02	1.18	1.30	0.97	0.82	0.64	0.86	0.26	0.23	0.22	b.d.l.	0.04	0.01	0.12	0.13	0.28	b.d.l.	b.d.l.	b.d.l.
H_2O#	3.50	3.44	3.50	3.28	3.23	3.36	3.31	3.39	3.25	3.59	3.61	3.61	3.69	3.68	3.69	3.72	3.77	3.65	3.78	3.79	3.78
–O=F	–0.01	–0.03	–0.01	–0.50	–0.55	–0.41	–0.35	–0.27	–0.36	–0.11	–0.10	–0.09	0.00	–0.02	0.00	–0.05	–0.05	–0.12	0.00	0.00	0.00
Total	100.25	100.09	100.87	100.12	100.69	100.16	100.86	100.40	100.67	100.20	100.52	100.10	101.10	102.16	101.39	99.90	100.79	100.36	100.15	100.42	100.27
apfu																					
Si	5.956	5.985	5.995	6.000	6.000	6.000	6.000	6.000	5.947	5.929	5.930	5.950	6.000	5.985	6.000	6.000	6.000	6.000	5.989	5.980	5.991
Ti	0.090	0.122	0.128	0.080	0.093	0.137	0.007	0.011	0.008	0.011	0.015	0.014	0.002	0.049	0.005	0.004	0.002	0.006	–	–	–
B #	3.000	3.000	3.000	3.000	3.000	3.000	3.000	3.000	3.000	3.000	3.000	3.000	3.000	3.000	3.000	3.000	3.000	3.000	3.000	3.000	3.000
Al	5.937	5.603	5.806	6.819	6.908	6.836	6.042	5.935	6.033	7.106	7.110	7.095	6.327	6.144	6.272	6.202	6.217	6.211	6.643	6.645	6.537
V^{3+}	0.001	0.006	0.001	–	–	–	–	–	–	–	–	–	0.009	0.008	0.009	–	–	–	–	–	–
Fe^{3+} *	0.104	0.189	0.000	0.046	0.050	0.062	0.098	0.000	0.000	0.000	0.000	0.000	0.004	0.000	0.000	0.217	0.242	0.344	0.000	0.000	0.000
Fe^{2+} *	2.123	2.283	2.232	0.000	0.000	0.000	0.572	0.562	0.920	0.875	0.844	0.852	1.055	1.255	1.098	0.000	0.000	0.000	0.187	0.187	0.183
Fe_{tot}	2.227	2.472	2.232	0.046	0.050	0.062	0.670	0.562	0.920	0.875	0.844	0.852	1.059	1.255	1.098	0.217	0.242	0.344	0.187	0.187	0.183
Mn^{2+}	0.042	0.048	0.136	0.070	0.063	0.069	0.116	0.041	0.087	0.089	0.090	0.096	0.010	0.011	0.008	0.001	0.007	0.023	0.019	0.015	0.015
Mg	0.746	0.765	0.647	0.354	0.302	0.351	1.891	2.303	1.865	0.237	0.240	0.233	1.464	1.450	1.497	2.213	2.083	2.008	1.989	2.000	2.111
Ca	0.048	0.074	0.051	0.404	0.424	0.417	0.218	0.254	0.255	0.085	0.079	0.080	0.057	0.139	0.071	0.129	0.062	0.112	0.000	0.000	0.000
Na	0.755	0.817	0.874	0.470	0.451	0.460	0.669	0.683	0.680	0.596	0.612	0.577	0.664	0.597	0.673	0.601	0.536	0.559	0.551	0.567	0.645
K	0.015	0.024	0.022	0.004	0.004	0.004	0.013	–	0.007	–	–	–	0.004	0.002	0.006	0.008	–	0.002	–	–	–
Li	0.000	0.000	0.054	1.631	1.584	1.544	0.274	0.148	0.140	0.753	0.770	0.760	0.129	0.097	0.112	0.363	0.449	0.408	0.172	0.172	0.163
F	0.016	0.038	0.011	0.583	0.641	0.482	0.422	0.326	0.445	0.130	0.119	–	–	0.021	0.005	0.060	0.064	0.140	–	–	–
Cl	0.000	0.000	0.000	0.000	0.000	0.000	0.000	0.000	0.000	0.000	0.000	0.000	0.000	0.000	0.000	0.000	0.000	0.000	0.000	0.000	0.000
OH#	3.984	3.962	3.989	3.417	3.359	3.518	3.578	3.674	3.555	3.870	3.881	3.890	4.000	3.979	3.995	3.940	3.936	3.860	4.000	4.000	4.000

* contents of Fe^{2+} and Fe^{3+} in formula were calculated based on stoichiometry and charge balance.
# Contents of B_2O_3, Li_2O and H_2O were calculated based on stoichiometry.


a
vac
Na+K
Ca
Dolní Bory
E-S-DB
L-D-DB
b
Al
Liddicoatite
Elbaite
Oxy-schorl, Foitite
Oxy-dravite, Magnesio-foitite
Schorl
Dravite
(Fe+Mn)50Al50
Mg50Al50
c
vac
Na+K
Ca
Bližná
E-LE-BL
L-D-BL
d
Al
Liddicoatite
Elbaite
Oxy-schorl, Foitite
Oxy-dravite, Magnesio-foitite
Schorl
Dravite
(Fe+Mn)50Al50
Mg50Al50
e
vac
Na+K
Ca
Tamponilapa
E-DS-TA
I-E-TA
L-D-TA
f
Al
Liddicoatite
Elbaite
Oxy-schorl, Foitite
Oxy-dravite, Magnesio-foitite
Schorl, Buergerite
Dravite
(Fe+Mn)50Al50
Mg50Al50

Tab. 4 Unit-cell parameters of dravite from studied localities compared to dravite from Forshammar, Sweden (Bačík et al. 2012), calculated average bond lengths in YO_6 and ZO_6 octahedra and ^{Z}Mg content with empirical equations.

	L-D-DB	L-D-Bl	L-D-Ta	Forshammar
a (Å)	15.933(3)	15.916(3)	15.913(2)	15.921(1)
c (Å)	7.1800(2)	7.1615(2)	7.1773(1)	7.157(1)
V (Å^3)	1578.6(2)	1571.1(3)	1574.1(2)	15175.05
Y-O (Å)	2.019	2.011	2.01	2.012(2.014)
Z-O (Å)	1.923	1.919	1.923	1.923(1.922)
^{Z}Mg (Å)	0.72	0.56	0.7	0.70(0.68)

vibration of Mg–O and Fe–O and the position of 238 cm^{-1} corresponds to the deformation vibration of O–Al–O. The sharp peak of the strips at the 369 cm^{-1} position represents a strong Al–O bond. Valence vibration B–O and strain vibration O–B–O correspond to position 757 cm^{-1} (Makreski and Jovanovski 2009). The strong vibration at position 1057 cm^{-1} refers to the valence vibration of the Si_6O_{18} ring. Deformation vibrations in the region of 3560–3500 cm^{-1} is caused by the presence of OH- (Reddy et al. 2007) and correspond to typical dravite (Fig. 7).

4.4. Powder XRD results

Unit-cell parameters of dravite from three localities (Tab. 4) are typical for tourmaline with a relatively very low Fe content, such as in tourmaline from Forshammar, Sweden (Bačík et al. 2012). Empirical equations based on the data from 37 tourmalines of the dravite-schorl series (dataset from Bačík 2015) allowed the calculation of average bond lengths at both octahedral sites based on the positive correlation of *a* with <*Y*–O> and *c* with <*Z*–O>. These are also typical for low-Fe dravites and very similar to dravite from Forshammar (Bačík et al. 2012). The empirical equation was used for the calculation (L-D-Ta) of ^{Z}Mg and the possible degree of Al–Mg disorder between octahedral sites. The (L-D-DB) and (L-D-Ta) samples are very similar, with 0.70–0.72 *apfu* ^{Z}Mg; the (L-D-Bl) sample displays a lower degree of Al–Mg disorder with 0.56 *apfu* ^{Z}Mg.

5. Discussion

5.1. Textural relations and mineral assemblages of late fibrous dravite

Late fibrous dravites from the individual localities differ in their size, morphology and color (Tab. 2). They vary from dark grey subparallel fibers (L-D-DB) (Fig. 2a), parallel to subparallel pale brown to colorless fibers (L-D-Ta) frequently oriented parallel with the *c*-axis of early dravite-schorl (E-DS-Ta) to very fine colorless to brownish hair-like aggregates in secondary vugs after early tourmaline (L-D-Ta) (Fig. 4a). The contact between early tourmaline is sharp in Dolní Bory N to gradual in the Bližná I and in Tamponilapa Ambany. Variations in color of fibrous tourmaline are typical in both Li-enriched pegmatites.

In the Dolní Bory N opal CT is closely associated (Fig.2) and fibers of dravite probably crystallized into open space subsequently filled by late opal. In the Bližná I pegmatite massive to fibrous overgrowths of dravite (L-D-Bl) evolve gradually from blue rather massive tourmaline via blue to colorless coarse-fibrous to fine-fibrous aggregate often developed into a host massive quartz and partly to K-feldspar (Fig. 3b). Solely in the Bližná I pegmatite, late dravite did not crystallized into an open vug and it is mostly enclosed in a massive quartz. We did not identify any minerals associated with late fibrous dravite which may provide more information about PTX-conditions in the localities. Accordingly, the textural relations (contact, orientation of fibers) of late fibrous dravite to early tourmaline as well as its fibrous morphology and color are rather distinct in the individual localities (Tab. 2). Sharp contacts and existence of the narrow intermediate zone (I-E-Ta) suggest rather overgrowing of early tourmalines although replacement textures also were found. An existence of intermediate tourmaline ((I-E-Ta) indicates more complex evolution in this locality. However, recognition of the textures related to overgrowing or to replacement and dissolution of early tourmaline is uneasy in many cases (Fig. 3b). In the Tamponilapa Ambany pegmatite and likely in Dolní Bory N fibrous tourmaline crystallized into open space.

5.2. Chemical composition of tourmalines

5.2.1. Early tourmalines – EMPA

The contents of major and minor elements in early tourmalines vary considerably (Fig. 5, Tab. 3). They include

⇦

Fig. 5 Compositional diagrams Na+K–Ca–vac. (a, c, e) and Al–Fe+Mn–Mg (b, d, f) of early and late tourmalines: **a, b –** Dolní Bory tourmalines; **c, d –** Bližná tourmalines; **e, f –** Tamponilapa tourmalines.

Mg-rich Al-poor schorl (E-S-DB) tending to bosiite composition from Dolní Bory N (Novák et al. 2017), Mg-enriched liddicoatite-elbaite (E-LE-Bl) from Bližná I and Ca,Fe-rich dravite and fluor-dravite to Mg-rich schorl (E-DS-Ta) from Tamponilapa Ambany. Early tourmaline (E-S-DB) from Dolní Bory N has rather low Al (5.13–5.69 *apfu*) and high to moderate Fe/Mg. So, external contamination of parental medium (pegmatite melt) from host serpentinite during emplacement and slightly after (Novák 2013) is evident. In the Bližná I pegmatite, elevated concentrations of Ca and moderate Mg in early Li-bearing tourmalines (liddicoatite to elbaite) associated with diopside and allanite in the (ii) elbaite-liddicoatite unit (Fig. 1a) indicate contamination from host rock evident chiefly in tourmalines from the (v) uvite-liddicoatite unit (Novák et al. 1999, 2012). The composition of Fe-rich elbaite (I-E-Ta) as a narrow zone developed locally between primary Fe-rich dravite and fluor-dravite to Mg-rich schorl (E-DS-Ta) and fibrous dravite to oxy-dravite (L-D-Ta) is similar to the liddicoatite–elbaite from Bližná I but has higher Fe/Mg ratio and lower Ca.

In the pegmatite Tamponilapa Ambany, elbaite-liddicoatite is a minor Li-mineral along with locally abundant spodumene. Also, its chemical composition with rather low contents of Mn differs from Li-tourmalines from typical elbaite-subtype pegmatites (e.g., Novák and Povondra 1995; Laurs et al. 1998) and is similar to spodumene-subtype pegmatites (Tindle et al. 2005). Primary tourmaline (E-DS-Ta) replaced by fibrous dravite is more primitive comparing primary tourmaline associated with garnet (Mg-poor schorl to Fe-rich elbaite) from central parts of the pegmatite body (Buřival and Novák 2018); however, both early tourmalines are Ca-enriched. At this locality, early Fe-rich dravite

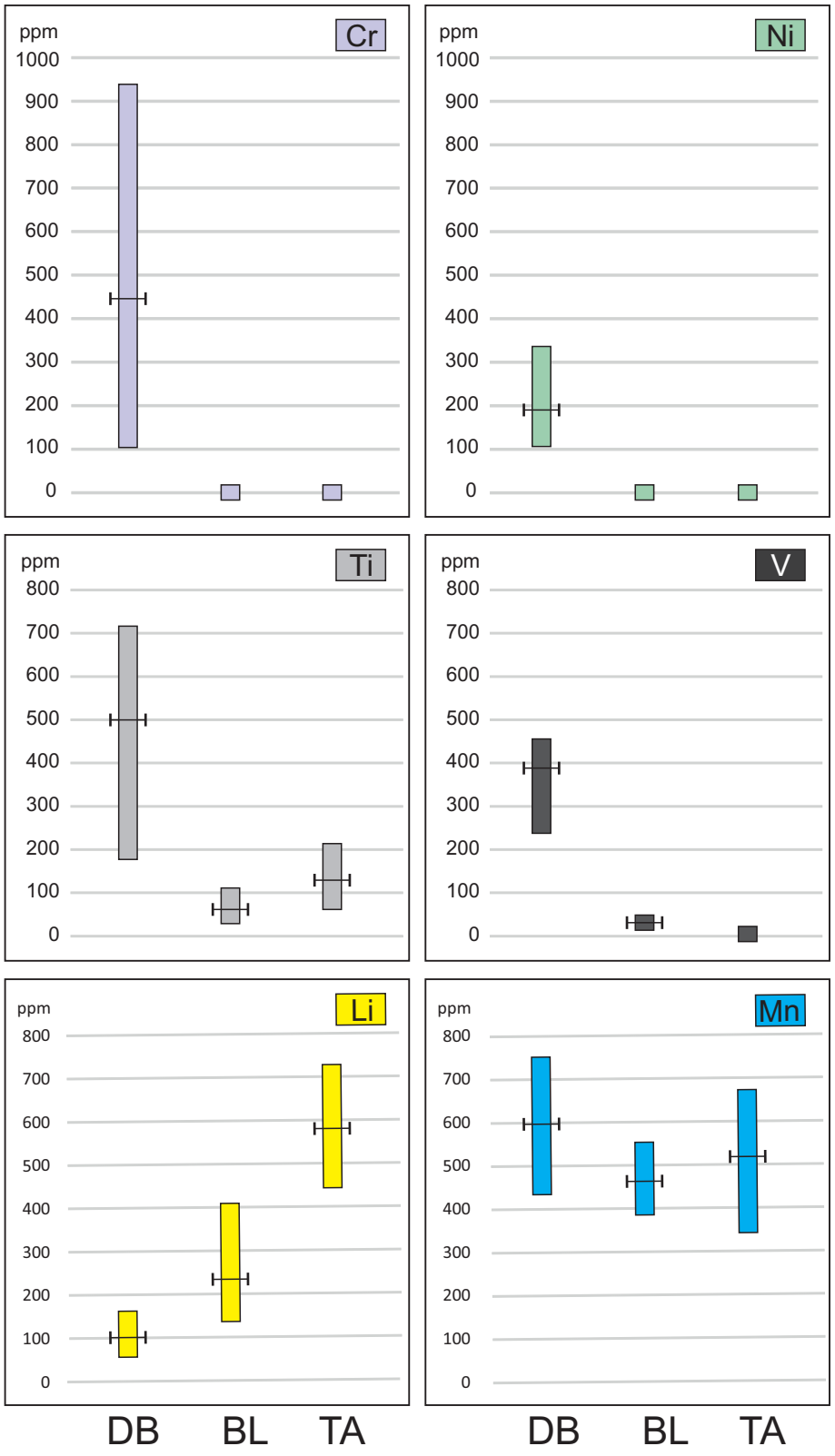


Fig. 6 Concentrations of selected trace elements in fibrous tourmalines through LA-IC-MS with average highlighted.

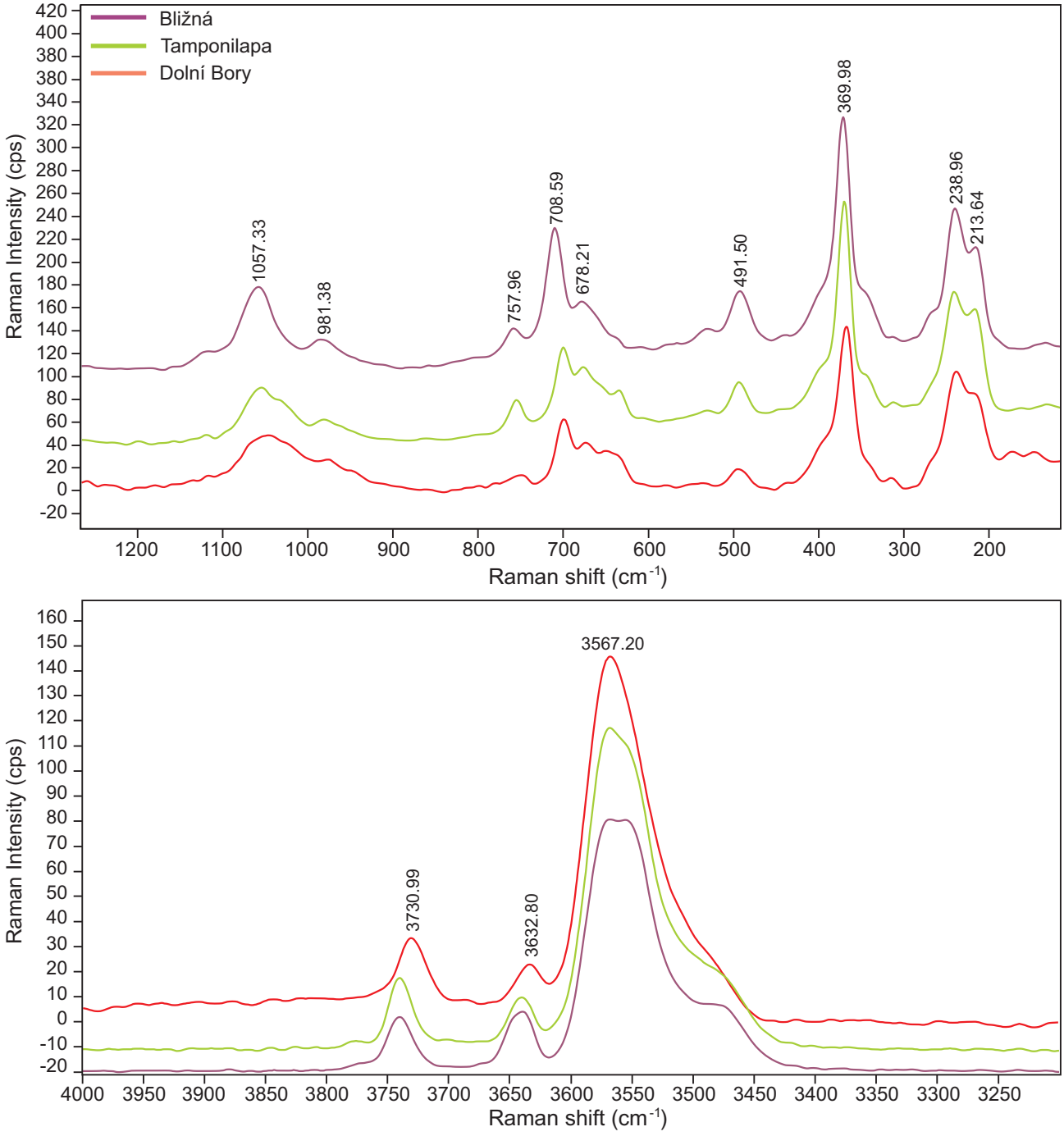


Fig. 7 Raman spectra of fibrous tourmalines.

and fluor-dravite to Mg-rich schorl (E-DS-Ta) is typically developed in albite close to the contact (Fig. 1b). It may reflect low degree of fractionation of tourmaline which crystallized close to the contact and was very likely also facilitated by early external Ca,Mg-contamination from the host rock (cf. Čopjaková et al. 2021). In general, the early tourmalines manifest degree of fractionation of the parental pegmatite and/or the host textural-paragenetic unit (Li-poor versus Li-enriched). Obvious contribution of early external contamination from host Ca,Mg-rich rocks with elevated contents of Mg and/or Ca in early tourmalines (Fig. 5) is also evident at all localities.

5.2.2. Late fibrous tourmalines – EMPA and LA-ICP-MS

Late fibrous tourmalines have quite similar chemical compositions at the examined pegmatites, and they cor-

respond to dravite, oxy-dravite and very rare magnesio-foitite (Fig. 5, Tab. 3); high Mg is typical as well as almost no F. Nevertheless, dravite from Dolní Bory N (L-D-DB) and Bližná I (L-D-Bl) have moderate Al (6.07–6.37 *apfu*) whereas dravite to oxy-dravite to very rare magnesio-foitite from Tamponilapa Ambany (L-D-Ta) are Al-enriched (6.42–6.77 *apfu*) (Fig. 5). Dravite from Bližná I (L-D-Bl) is slightly Ca-enriched (0.04–0.13 *apfu*) and dravite from Dolní Bory N (L-D-DB) evidently Fe-enriched (0.97–1.26 *apfu*) (Fig. 5). The elevated contents of some elements (Al, Fe, Mg, and Ca) in late fibrous tourmalines are typically related to the compositions of their early tourmalines (Fig. 5). Compared with the relevant early tourmalines, all late fibrous tourmalines show a higher vacancy in the *X*-site position, lower contents of F and higher Mg (Fig. 5). In general, the compositions of fibrous dravite from all localities are similar and differences related to the compositions of their relevant early tourmalines are evident (Fig. 5).

Elevated contents of the trace elements (Cr, Ni, Ti and V) in the Dolní Bory N pegmatite (Fig. 6) reflect very well the composition of host serpentinite from the Bory Granulite Massif. Elevated concentrations of Li in fibrous tourmalines from Li-bearing pegmatites with liddicoatite–elbaite (Bližná I, Novák et al. 1999, 2012), and spodumene + elbaite–liddicoatite (Tamponilapa Ambany, Novák et al. 2025) are evident; however, in the Tab. 3 the calculated Li is not consistent with the LA-ICP-MS data at Tamponilapa Ambany (Fig. 6).

5.3. Potential sources of the individual elements and origin of fibrous dravite

The concentrations of trace elements in late fibrous tourmalines discussed above are evidently related to the composition of their host rocks chiefly in the Dolní Bory N pegmatite. External fluids from the host rocks were participated and likely facilitated crystallization of late fibrous dravite. They sourced Mg at all examined localities but also the trace elements (Ni, Cr, V) in the Dolní Bory N pegmatite cutting serpentinite body. Alteration of early biotite supposed as a source of Fe and Mg in fibrous tourmaline from the Rosina pegmatite, Piero in Campo, Elba by Andreozzi et al. (2025) is not probable. Biotite is absent in the Bližná I pegmatite and elevated concentrations of Cr, Ni and V in fibrous dravite (Fig. 6) from the Dolní Bory N pegmatite rather indicate contamination from the host rock. Blue to colorless dravite overgrowing early liddicoatite–elbaite in Bližná I evolved from massive to fibrous habitus into a massive quartz; the contamination from host rock is indicated by elevated contents of Mg in early liddicoatite–elbaite (E-EL-Ta) from (v) uvite–liddicoatite unit and also by the occurrence of diopside and allanite in the (ii) elbaite–liddicoatite unit (Novák et al. 1999). In the Tamponilapa Ambany pegmatite fibrous dravite was found only in early tourmaline occurring close to the upper contact. Biotite randomly distributed in the pegmatite body is mostly fresh or partly replaced by blue fibrous Fe,Mn-elbaite (Buřival and Novák 2018) and/or ferro-holmquistite (Novák et al. 2025). Consequently, some cations (Mg, Ni, Cr, V) were evidently supplied from Mg- and Ca,Mg-rich host rock; low contents of Ca in fibrous dravite were very likely constrained by the crystal structure (see below). Further dominant cations (Si, Al, Fe, Na) come from altered/dissolved early tourmaline and from B-enriched internal fluids as is manifested by the existence of tourmaline-rich contact zones in the Bližná I (Fig. 1a) and Tamponilapa Ambany pegmatites.

Elevated concentrations of Li in fibrous tourmalines from both Li-bearing pegmatites (Bližná I, Tamponilapa Ambany; Fig. 6) indicate that Li may have been sourced from early tourmalines. In the Bližná I pegmatite late blue dravite (L-D-Bl) may have replaced early liddicoatite-elbaite (E-LE-Bl). However, participation of Li-enriched residual fluids is more likely chiefly in Tamponilapa, where late fibrous Fe,Mn-elbaite replaced garnet (Buřival and Novák 2018) and ferro-holmquistite biotite (Novák et al. 2025), and, moreover, early parental Fe-rich dravite to Mg-rich schorl (E-DS-Ta) is very likely Li-poor. Also, Li,F-enriched dravite–uvite + elbaite–liddicoatite from the contact zone in Bližná I and holmquistite ± spodumene in the contact zone from the Tamponilapa Ambany pegmatite manifest that the residual fluids were Li-enriched.

In the Dolní Bory N pegmatite, grey fibrous dravite is ongrowing large grain of black schorl with sharp contact (Fig. 2a) and rare secondary tourmaline after biotite was found at this locality as well (Macek 2012); hence, B-enriched fluids very likely of internal origin supplied most B. Massive blue dravite is growing on liddicoatite-elbaite at Bližná I and evolves to blue to colorless fibrous dravite both enclosed in a massive quartz (Fig. 3); no other secondary tourmaline has been found in this pegmatite (Novák et al. 1999). High activity of B-rich fluids in the (v) uvite–liddicoatite unit is manifested by the existence of tourmaline-dominant contact zone developed only between the (v) uvite–liddicoatite unit and host marble (Fig. 1a) and internal fluids are evident source of B in this locality. Primary altered tourmaline may have been the source of B in the Tamponilapa Ambany pegmatite, where fibrous dravite to oxy-dravite grows into open vugs, up to several cm^3 in size, after evidently dissolved early tourmaline within a single tourmaline aggregate. However, secondary Li-bearing tourmaline (Fe,Mn-elbaite) ± ferro-holmquistite replacing garnet and biotite at this locality indicates Li-enriched residual fluids to be a potential source of B as well. Consequently,

internal fluids are dominant source of B although both residual fluids and the altered early tourmalines supplied B chiefly in the Tamponilapa Ambany pegmatite and their participation may have varied in space and time as well as within the individual localities.

Recognition of the origin of fibrous tourmalines by a direct replacement of early tourmaline or overgrowing of an altered early tourmaline is mostly not evident from the textural relations (Figs 2, 3, 4). High Mg contents as well as the concentrations of some trace elements (Fig. 6) in all fibrous dravites manifest significant role of external fluids from host rock chiefly in Dolní Bory N and the pegmatite systems were evidently open during growing at least part of fibrous tourmalines. However, compositional similarities of early tourmalines and the relevant late fibrous tourmalines (Fig. 5) manifest that late fibrous dravite mainly from the Tamponilapa Ambany pegmatite replaced early tourmaline or fluids originated during breakdown/dissolution of early tourmaline participated on its origin. However, existence of contact reaction zones around the pegmatite Bližná I (Fig. 1a) and Tamponilapa Ambany shows that internal fluids in the pegmatites were enriched in the relevant elements (Si, Al, Fe, Na). The existence of intermediate zone (I-E-Ta) (Fig. 4) often developed between early tourmaline (E-DS-Ta) and late dravite (L-D-Ta) typically parallel with the *c*-axis of early tourmaline rather suggests polyphase process when dominant activity of internal residual Li,B-enriched fluids was followed by external Mg-enriched fluids.

5.4. Possible crystal growth structural constraints

The similar chemical compositions of late fibrous dravite to oxy-dravite tending to magnesio-foitite from granitic pegmatites with different degrees of fractionation but similar host rocks (Mg-rich and Mg,Ca-rich), and from a variety of low-grade metamorphic rocks, hydrothermal systems and veins and open vugs in granitic pegmatites (Dutrow and Henry 2016 and references therein) suggest that crystal-structural constraints may have played a significant role.

Tourmalines with very thin, acicular, and almost fibrous crystals share many interesting common features but also some differences. Firstly, tourmalines with a high Mg/(Mg+Fe) and increased Al content very often tend to form acicular to fibrous crystals (Bačík et al. 2015), although fibrous foitites are also relatively common (Dutrow and Henry 2016). Another common feature is the *X*-site occupancy. At present, all known fibrous tourmalines from worldwide localities and petrologic environments belong to the *X*-site vacant or alkali-group tourmalines (Dutrow and Henry 2016).

This fibrous habitus is very typical for magnesio-foitite, also at its type locality of Kyonosawa, Japan, where it is rich in Al (7.42 *apfu*) and Mg (1.44 *apfu*) but Fe-poor with only 0.13 *apfu* and Ca below the detection limit of EPMA (Hawthorne et al. 1999). Similar Fe- and Ca-poor magnesio-foitites can be found in several localities worldwide, such as the Athabasca Basin, Saskatchewan, Canada (Rosenberg and Foit 2006), Kapka and Tisovec, Slovakia (Bačík et al. 2015). An example of thin-prismatic dravite can be found on the talc-magnesite deposit in Gemerská Poloma, Slovakia, with high Mg content (≤2.77 *apfu*), very low Fe content (≤0.14 *apfu*), Al content in the range of 5.97 and 6.27 *apfu* and, *X*-site vacancy ≤0.17 *pfu* and Ca below 0.05 *apfu* (Bačík et al. 2011) or at the Brumado magnesite deposit in Brazil with the compositions in the trend from dravite to magnesio-foitite with Mg in the range of 2.23–2.44 *apfu*, Al ≤6.66 *apfu* and Fe below 0.49 *apfu* (Modreski et al. 1997). The *X*-site vacancy is strongly variable, from 0.23 to 0.78, but Ca is always ≤0.11 *apfu* (Modreski et al. 1997). The studied samples show many similarities to most acicular to fibrous tourmalines. Dravites from Dolní Bory N and Bližná I pegmatites have lower Al content, ≤6.40 *apfu*, whereas the sample from Tamponilapa has distinctly higher Al but below 7 *apfu*. In contrast, Bližná I and Tamponilapa Ambany are similar in their very low Fe contents, whereas the sample from Dolní Bory N is slightly enriched in Fe. All samples are poor in Ca and the *X*-site vacancy varies between 0.3 and 0.5 *pfu*.

The intriguing connection between the crystal habit and its crystal chemistry has already been described previously and is also consistent with the studied samples. Enrichment in Al above 6.00 *apfu* appears to be one of the most common compositional features of acicular to fibrous tourmalines (Bačík et al. 2015). The Al^{3+} cation strongly prefers the *Z*-site, which forms interconnected chains of octahedra parallel to *c*. The distribution of Mg is influenced by the Al-Mg disorder (Hawthorne et al. 1993; Ertl et al. 2010; Bosi et al. 2010). Based on the structural and compositional data of the schorl-dravite series, statistically, at least 30% and up to 97 % of Mg is usually distributed at the *Z*-site (Bačík 2015). The studied samples have increased Al content, although not exceeding 6.91 *apfu* but the proportion of ^{Z}Mg calculated from the unit-cell parameter *c* indicates that, in accordance with the general trend in schorl-dravite series, 30–50 % of Mg is likely located at the *Z*-site. Based on the calculated bond lengths, Al is a strongly *Z*-preferring cation, and Mg has a mixed preference between the *Y*- and *Z*-sites (Bačík and Fridrichová 2021). Therefore, their high contents may favour preferential structural development of the ZO_6 chains in the *c*-direction, resulting in the prolongation of crystals, whereas a lower content of strongly *Y*-preferring cations, mainly Fe^{2+}, may be associ-

ated with a favoured structural development perpendicular to the elongation direction due to reduced formation of YO_6 octahedra triplets (Bačík et al. 2015). Consequently, in the Al- and Mg-rich environment, it can be presumed that polymerization of the ZO_6 octahedral chains may be favoured relative to growth in the perpendicular direction, resulting in the acicular to fibrous habitus.

This is also in accordance with the low Ca contents, which are generally observed in fibrous tourmalines (Dutrow and Henry 2016). The presence of divalent cation at the *X*-site requires stronger *X*–O2 bonds necessary for the accommodation of Ca^{2+}. At the same time, the *Y*–O2 bond must be weaker. Therefore, tourmalines with divalent cations strongly dominant at the *Y*-site, forming weaker bands in general, are preferred to contain Ca^{2+} at the *X*-site. Moreover, it was evidenced that there is a positive correlation between total Al and *Y*–O2 bond strength (Tab. 4, Bačík 2015, 2018). It is a general property of Al-rich tourmalines to have strong *Y*–O2 bonds and, therefore, low residual bond valence available for *X*–O2 (Bačík et al. 2015). Consequently, significant Ca contents would not generally be expected in Al-rich fibrous tourmalines, although we can expect elevated activity of Ca in fluids from the Bližná I and Tamponilapa Ambany pegmatites cutting Ca,Mg-rich metacarbonate rocks.

As is generally known, the rate and time for crystallization depend on the temperature and cooling rate. Most acicular and fibrous tourmalines are developed in environments with relatively low temperatures (~150–400 °C) and pressures below 3 kbar (Dutrow and Henry 2016). During rapid crystallization, crystal growth may become increasingly anisotropic, favouring elongation along the faster-growing direction and resulting in the development of acicular to fibrous tourmaline crystals (Bačík et al. 2015). The rate of crystallization is likely fluid-controlled and is usually connected to late, fluid-driven processes (Dutrow and Henry 2016).

6. Conclusions

Late fibrous tourmalines (dravite, oxy-dravite > magnesio-foitite) from granitic pegmatites hosted in Mg- and Ca,Mg-rich rocks record very well the chemical composition of their host rocks including trace elements (Cr, Ni, V) as well as the composition of the associated early tourmalines. It manifests that both external fluids and internal residual fluids, as well as the chemical compositions of early replaced/dissolved tourmalines, have played a substantial role in the composition of the examined late fibrous tourmalines.

Boron was provided chiefly by residual pegmatite fluids, which are typically B-enriched. It is documented very well at the examined localities Bližná I (Novák et al. 1999; Krmíček et al. 2021) and Tamponilapa Ambany (Buřival and Novák 2018; Novák et al. 2025) by the existence of tourmaline-rich exocontact zones. However, also the altered/dissolved early tourmaline which also provided some essential cations (e.g., Si, Al, Fe) for newly formed fibrous dravite to oxy-dravite may have supplied part of B.

The textural relations between early and late fibrous tourmalines are complex and do not allow to reliably define their origin – direct replacement of early tourmaline or its overgrowing. However, early tourmaline alteration is evident chiefly in Tamponilapa Ambany and dissolution of early tourmaline proceeded later overgrowing process. Origin of late fibrous tourmalines is a complex process which may include dissolution of early tourmaline, its direct replacement and overgrowing. Participation of these processes may have varied in space and time as well as within the individual localities.

The fibrous to acicular texture of late tourmalines, which crystallized from low-T aqueous fluids in a fluid-filled space, is controlled chiefly by crystal-structural constraints (high Al content and its preference for the *Z* site) and rate of crystallization. Late fibrous tourmalines may serve as valuable indicators of the fluid composition during late stages of tourmaline-bearing systems evolution.

Acknowledgements: The authors thank two anonymous reviewers for constructive criticism that significantly improved the manuscript. We also appreciate consultations with Lenka Skřápková and Jiří Toman for taking selected macro photos. This work was supported by internal grant of National Museum, Prague 2011/05/IG-PM to IM, by OP RDE [grant number CZ.02.1.01/0.0/0.0/16_026/0008459 (Geobarr) from the ERDF] for MN and APVV-18-0065 and VEGA 1/0671/26 projects to PB.

References

Andreozzi GB, Di Giuseppe D, Gualtieri AF, Scognamiglio V, Fornasini L, Bersani D, Giovanardi T, Lugli F, Pezzotta F (2025) Fibrous tourmaline from San Piero in Campo (Elba, Italy). Eur J Mineral 37(4): 437–453

Aurisicchio C, Ottolini L, Pezzotta F (1999) Electron- and ion microprobe analyses, and genetic inferences of tourmalines of the foitite–schorl solid solution, Elba Island (Italy). Eur J Mineral 11: 217–226

Bačík P (2015) Cation ordering in octahedral sites in tourmalines of schorl–dravite series. Canad Mineral 53: 571–590

Bačík P (2018) The crystal-chemical autopsy of octahedral sites in Na-dominant tourmalines: octahedral metrics

model unconstrained by the Y, Z-site disorder assignment. J Geosci 63: 137–154

Bačík P, Fridrichová J (2021) Cation partitioning among crystallographic sites based on bond-length constraints in tourmaline-supergroup minerals. Am Mineral 106: 851–861

Bačík P, Dianiška I, Števko M, Sečkár P (2011) Brown acicular dravite from talc–magnesite deposit Gemerská Poloma (Gemeric Superunit, Slovakia). Bull Mineral Petrol 19: 164–170 (in Slovak)

Bačík P, Uher P, Ertl A, Jonsson E, Nysten P, Kanický V, Vaculovič T (2012) Zoned REE-enriched dravite from a granitic pegmatite in Forshammar, Bergslagen province, Sweden: An EMPA, XRD and LA-ICP-MS study. Canad Mineral 50: 825–841

Bačík P, Ertl A, Števko M, Sečkár P, Giester G (2015) Acicular zoned tourmaline (magnesio-foitite to foitite) from a quartz vein near Tisovec, Slovakia: The relationship between crystal chemistry and acicular habitus. Canad Mineral 53: 221–234

Bosi F, Balić-Žunić T, Surour AA (2010) Crystal structure analyses of four tourmaline specimens from the Cleopatra's Mines (Egypt) and Jabal Zalm (Saudi Arabia), and the role of Al in the tourmaline group. Am Mineral 95: 510–518

Buřival Z, Novák M (2018) Secondary blue tourmaline after garnet from elbaite-subtype pegmatites; implications for source and behaviour of Ca and Mg in fluids. J Geosci 63(2): 111–122

Čopjaková R, Prokop J, Novák M, Losos Z, Gadas P, Škoda R, Holá M (2021) Hydrothermal alteration of tourmaline from pegmatitic rocks enclosed in serpentinites: Multistage processes with distinct fluid sources. Lithos 380: 105823, https://doi.org/10.1016/j.lithos.2020.105823

Cox R, Armstrong RA, Ashwal LD (1998) Sedimentology, geochronology and provenance of the Proterozoic Itremo Group, central Madagascar, and implications for pre-Gondwana palaeogeography. J Geol Soc 155(6): 1009–1024

Dutrow BL, Henry DJ (2000) Complexly zoned fibrous tourmaline, Cruzeiro mine, Minas Gerais, Brazil: a record of evolving magmatic and hydrothermal fluids. Canad Mineral 38: 131–143

Dutrow BL, Henry DJ (2016) Fibrous tourmaline: a sensitive probe of fluid compositions and petrologic environments. Canad Mineral 54(1): 311–335

Ertl A, Mali H, Schuster R, Körner W, Hughes JM, Brandstätter F, Tillmanns E (2010) Li-bearing, disordered Mg-rich tourmalines from the pegmatite-marble contact from the Austroalpine basement units (Styria, Austria). Mineral Petrol 99: 89–104

Felch M, Falster AU, Simmons WB (2016) Iron-bearing pollucite and tourmaline replacement of garnet in the garnet line in the Mt. Mica and Havey pegmatites, Western Maine. Canad Mineral 54: 1071–1086

Gadas P, Novák M, Staněk J, Filip J, Vašinová Galiová M (2012) Compositional evolution of zoned tourmaline crystals from pockets in common pegmatites of the Moldanubian Zone, Czech Republic. Canad Mineral 50: 895–912

Hawthorne FC, MacDonald DJ, Burns PC (1993) Reassignment of cation site occupancies in tourmaline: Al–Mg disorder in the crystal structure of dravite. Am Mineral 78: 265–270

Hawthorne FC, Selway JB, Kato A, Matsubara S, Shimizu M, Grice JD, Vajdak J (1999) Magnesiofoitite, $\square(Mg_2Al)Al_6(Si_6O_{18})(BO_3)_3(OH)_4$, a new alkali-deficient tourmaline. Canad Mineral 37: 1439–1443

Henry DJ, Dutrow BL (2012) Tourmaline at diagenetic to low-grade metamorphic conditions: Its petrologic applicability. Lithos 154: 16–32

Krmíček L, Novák M, Trumbull RB, Cempírek J, Houzar S (2021) Boron isotopic variations in tourmaline from metacarbonates and associated calc-silicate rocks from the Bohemian Massif: Constraints on boron recycling in the Variscan orogen. Geosci Front 12(1): 219–230

Laugier J, Bochu B (2011) LMGP-Suite of Programs for the Interpretation of X-ray Experiments.

Laurs BM, Dilles JH, Wairrach Y, Kausar AB, Snee LW (1998) Geological setting and petrogeneseis of symmetrically zoned, miarolitic granitic pegmatites at Stak Nala, Nanga-Parbat – Haramosh massif, northern Pakistan. Canad Mineral 36: 1–47

Macek I (2012) Late tourmalines and thein unusual compositional trends from granitic pegmatites of the Bohemian Massif. MS Master Thesis, Masaryk University Brno, pp 1–64 (in Czech)

Makreski P, Jovanovski G (2009) Minerals from Macedonia XXIII. Spectroscopic and structural characterization of schorl and beryl cyclosilicates. Spectrochim Acta, Part A 73: 460–467

Merlet C (1994) An accurate computer correction program for quantitative electron probe microanalysis. Microchim Acta 114/115: 363–376

Modreski PJ, Foord EE, Barbosa CP (1997) Crystal chemistry of uvite-dravite from the Brumado magnesite deposits, Bahia, Brazil. In: Tourmaline 1997 International Symposium on Tourmaline, Abstract Volume, 59–60

Moine B, Nédeléc A, Ortega E (2014) Geology and metallogeny of the Precambrian basement of Madagascar, J African Earth Sci 94: 1–8

Moore JN, Christenson B, Browne PRL, Lutz SJ (2004) The mineralogic consequences and behavior of descending acid-sulfate waters: an example from the Karaha–Telaga Bodas geothermal system, Indonesia: Canad Mineral 42: 1483–1499

Němec D (1989) Chemical composition of tourmaline in pegmatites of the Jihlava Massif (Western Moravia, ČSSR). Chem Erde 49: 317–340

Novák M (1998) Fibrous blue dravite; an indicator of fluid composition during subsolidus replacement processes in Li-poor granitic pegmatites in the Moldanubicum, Czech Republic. J Czech Geol Soc 43: 24–30

Novák M (2013) Contamination processes in complex granitic pegmatites. In: Simmons WB, Webber KL, Falster AU, Roda-Robles E, Hanson SL, Márquez-Zavalía MF, Galliski M (eds) PEG 2013: The 6th International Symposium on Granitic Pegmatites. Rubellite Press, New Orleans, pp 100–103

Novák M, Povondra P (1995) Elbaite pegmatites in the Moldanubicum: a new subtype of the rare-element class. Mineral Petrol 55: 159–176

Novák M, Taylor MC (2000) Foitite: Formation during late stages of evolution of granitic pegmatites at Dobrá Voda, Czech Republic and Pala, California, U.S.A. Canad Mineral 38: 1399–1408

Novák M, Selway JB, Černý P, Hawthorne FC, Ottolini L (1999) Tourmaline of the elbaite–dravite series from an elbaite-subtype pegmatite at Bližná, southern Bohemia, Czech Republic. Eur J Mineral 11: 557–568

Novák M, Škoda R, Gadas P, Krmíček L, Černý P (2012) Contrasting origins of the mixed (NYF+LCT) signature in granitic pegmatites, with examples from the Moldanubian Zone, Czech Republic. Canad Mineral 50: 1077–1094

Novák M, Prokop J, Losos Z, Macek I (2017) Tourmaline, an indicator of external Mg-contamination of granitic pegmatites from host serpentinite; examples from the Moldanubian Zone, Czech Republic. Mineral Petrol 111: 625–641

Novák M, Gadas P, Pezzotta F, eds (2025) Field trip Guidebook Sahatany Valley Conference. Tourmaline 2025 Antsirabe, Madagascar, pp 1–55

Pezzotta F, Hawthorne FC, Cooper MA, Teertstra DK (1996) Fibrous foitite from San Piero in Campo, Elba, Italy. Canad Mineral 34(4): 741–744

Radková P, Novák M, Cempírek J, Houzar S, Škoda R (2021) Amphibole and pyroxene as indicators of alkaline conditions in banded carbonatite-like marbles from Bližná, Český Krumlov Unit, Moldanubian Zone. J Geosci 66(4): 243–262

Ranorosoa N (1986) Etude minéralogique et microthermométrique des pegmatites du champ de la Sahatany – Madagascar. PhD Thesis, University Paul Sabatier, Toulouse. pp 1–223

Reddy BJ, Fost RL, Martens WN, Wain DL, Kloprogge JT (2007) Spectroscopic characterization of Mn-rich tourmalines. Vib Spectrosc 44: 42–49

Rosenberg PE, Foit FF Jr (2006) Magnesiofoitite from the uranium deposits of the Athabasca Basin, Saskatchewan, Canada. Canad Mineral 44: 959–965

Schulmann K, Lexa O, Janoušek V, Lardeaux JM, Edel JB (2014) Anatomy of a diffuse cryptic suture zone: an example from the Bohemian Massif, European Variscides. Geology 42(4): 275–278

Staněk J (2009) Minerals from Bory and Cyrilov near Velké Meziříčí. The Bory village, pp 1–102 (in Czech)

Tindle AG, Selway JB, Breaks FW (2005) Liddicoatite and associated species from the McCombe spodumene-subtype rare-element granitic pegmatite, northwestern Ontario, Canada. Canad Mineral 43(2): 769–793

Van Den Bleeken G, Corteel C, Van Den Haute P (2007) Epigenetic to low-grade tourmaline in the Gdoumont metaconglomerates (Belgium): A sensitive probe of its chemical environment of formation. Lithos 95: 165–176

Warr LN (2021) IMA-CNMNC approved mineral symbols. Mineral Mag 85: 291–320